



HAL
open science

Agglomeration in Solid Propellants loaded with inert particles - Study of physical phenomena using shadowgraphy image processing

Thomas Decker, Robin Devillers, Stany Gallier

► To cite this version:

Thomas Decker, Robin Devillers, Stany Gallier. Agglomeration in Solid Propellants loaded with inert particles - Study of physical phenomena using shadowgraphy image processing. EUCASS 3AF 2022, Jun 2022, Lille, France. 10.13009/EUCASS2022-4371 . hal-04020867

HAL Id: hal-04020867

<https://hal.science/hal-04020867>

Submitted on 9 Mar 2023

HAL is a multi-disciplinary open access archive for the deposit and dissemination of scientific research documents, whether they are published or not. The documents may come from teaching and research institutions in France or abroad, or from public or private research centers.

L'archive ouverte pluridisciplinaire **HAL**, est destinée au dépôt et à la diffusion de documents scientifiques de niveau recherche, publiés ou non, émanant des établissements d'enseignement et de recherche français ou étrangers, des laboratoires publics ou privés.

Agglomeration in Solid Propellants loaded with inert particles – Study of physical phenomena using shadowgraphy image processing

*Thomas Geoffrey DECKER**, *Robin William DEVILLERS*** and *Stany GALLIER****

,DMPE, ONERA, Université Paris Saclay, Palaiseau, F-91123*

thomas.decker@onera.fr · robin.devillers@onera.fr

**** ArianeGroup, 9 Rue Lavoisier, 91710 Vert-le-Petit, France*

stany.gallier@ariane.group

Abstract

New algorithms to study agglomeration in a solid propellant composition loaded with inert particles are presented. Shadowgraphy images are acquired using a high-speed set-up at ONERA. The composition containing inert particles is studied at three different pressure levels. Single particles and aggregates are detected on the surface and in the gas flow. Various metrics are considered in order to expose the effect of pressure on agglomeration such as residence time on the surface and initial acceleration in the gas flow. It is very promising to provide quantitative data that could be compared with future simulated agglomeration data.

1. Introduction

Solid Rocket Motors (SRM) burn solid propellant and are widely used in both military and civilian applications because of their many benefits. They are extremely reliable, require few maintenance and can be used at any moment. A solid propellant is a solid material used to generate thrust by its combustion. It is composed of a fuel and an oxidizer. The two components can be chemically bound (homogeneous propellant) or distinctive (composite propellant). Composite propellants are mainly used because of their better propulsive performances. The classic mixture fuel/oxidizer is HTPB (Hydroxyl-terminated PolyButadiene) / AP (Ammonium Perchlorate). Aluminum particles are added to increase performances with the additional heat release. While the fuel and the oxidizer burn at the surface, the aluminum particles added to the solid propellant burn in the gas flow produced by the fuel/oxidizer combustion. The aluminum combustion starts when the passivating alumina layer starts to liquefy and exposes the aluminum to the surrounding gas above the propellant burning surface.

But a large portion of the initial aluminum particles do not leave the surface of the propellant as individual particles, they are subject to agglomeration. The particles bind together through sintering or coalescence [1], forming aggregates. Aluminum surface agglomeration is limited by two phenomena: aggregates leave the propellant surface because of the drag force applied by the gas flow or because of the initiation of the aluminum combustion. Agglomeration results in bigger aluminum droplets burning in the gas flow. The increase of the burning droplets has many consequences: incomplete burning (for short motors), two-phase flow losses [2, 3], alumina slag formation [4], effects on instabilities [5, 6], etc. All those consequences directly depend on the size of the aluminum droplets.

The study of the increase in droplet size due to agglomeration has been a focus for various decades. Experimental studies [7–10] use particle collection as a method. The droplets are collected thanks to a liquid bath. Their size are measured afterwards. Correlations to estimate agglomeration proportions and size [11–14] have been established based on experimental studies. Agglomeration models have also been investigated. Some are based on geometric entities called pockets [15, 16]. Others are stochastic models [17–19] using a random repartition of the granular components of the solid propellant, called a packing [20], based on the real size distributions of the AP and Al particles. Stochastic models all include geometric effects and some include further agglomeration physics such as ignition. Direct Numerical Simulations (DNS) have recently been developed [21] but contain limited agglomeration physics, partially due to the lack of understanding of the underlying phenomena.

New experimental visualization setups have been developed in order to study the physics of agglomeration, shadowgraphy is one of them [22]. Shadowgraphy using a high-speed camera provides accurate details of the propellant surface during combustion, with the metal particles agglomerated on it.

AGGLOMERATION IN SOLID PROPELLANTS LOADED WITH INERT PARTICLES

Various works [22–24] have been focused on the study of propellant containing inert particles instead of aluminum particles. They are easier to study for various reasons (no smoke generated by the particles, no size modification over time for the targeted particles, . . .), and the aggregates are still visible above the surface. Studying the inert particles agglomeration can provide information of the agglomeration mechanisms in order to model it for aluminum. Image-processing algorithms [22–24] have already been developed in order to detect the objects (particles and aggregates) on the surface of the propellant and in the gas flow. The study presented here focuses on physical analyses of the behavior of those objects on the surface and in the gas. More specifically, the residence time on the surface and the acceleration in the gas flow are estimated and show variations with the pressure in the combustion chamber.

2. Experimental data

The shadowgraphy set-up is presented in figure 1 [22]. A solid propellant sample is placed inside a combustion chamber. It is ignited by a powerful CO₂ laser at 10.6 μ m. An extended light source illuminates the combustion chamber. It is focused with a lens in order to generate a beam that is brighter than the combustion gas generated by the combustion. An entrance grid is also included in order to reduce the depth of the measurement volume. A high-speed camera acquires images with a frequency of 7500Hz, the images are 1280 pixels wide and 800 pixels high. The spatial resolution of the images is around 3 μ m/pixel.

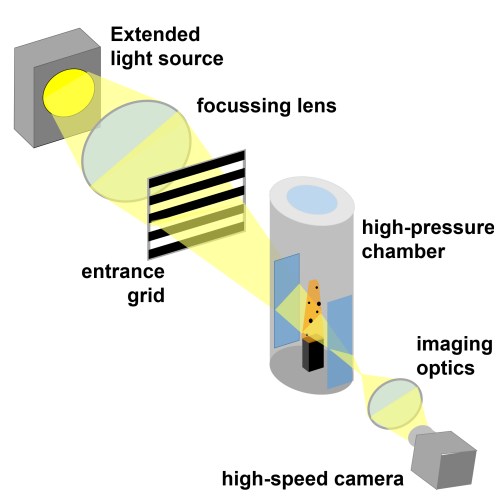


Figure 1: Shadowgraphy set-up [22].

One solid propellant composition is studied. The propellant is composed of AP/HTPB mixture, loaded with additional ceramic particles made of a ZrO₂, SiO₂ and Al₂O₃ mixture [22, 23, 25]. The composition includes AP particles with three diameter ranges (fine, medium and coarse AP). The targeted inert particles have a size distribution with a single peak around the averaged diameter of 34 μ m, representative of typical aluminum particles in solid propellants. The study is focused on three initial nitrogen pressures: 1, 3, and 10 bars.

3. Automatic image processing

The present section summarize the image-processing algorithms that are used. More details can be found in [24].

3.1 Automatic detection of the burning surface

The first step consist in automatically detecting the surface of the burning solid propellant sample, including the particles and aggregates that are still stuck on it. A surface-detection algorithm of detection has been developed previously [22, 23] based on the Chan-Vese active contour [26]. It was found to be more precise than a thresholding or other active contour [22, 23]. Figure 2 shows a shadowgraphy image with the surface detected by the active contour algorithm plotted in white. Particles and aggregates are attached to the surface of the propellant.

AGGLOMERATION IN SOLID PROPELLANTS LOADED WITH INERT PARTICLES

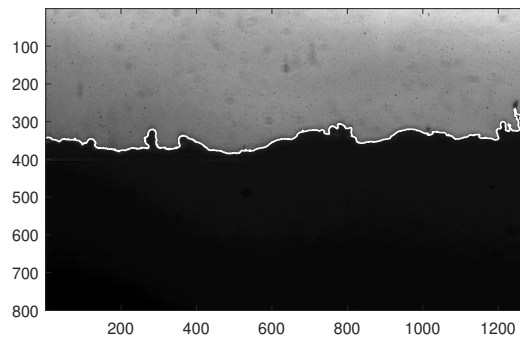


Figure 2: Shadowgraphy image of a burning propellant sample. The surface is plotted in white, as detected from the active contour algorithm.

3.2 Automatic detection of objects on the surface and in the gas

The automatic detection of particles and aggregates on the surface is studied in more details in [24]. The curvature of the surface using different Gaussian filters is calculated (approach inspired by [27]), the portions with high curvature correspond to particles and aggregates. They are detected with a couple of criteria based on the detections size and protuberance. The detection method was found able to provide very good detection performances (more than 80% of the particles and aggregates are automatically detected [24]).

A tracking of the objects on the surface was developed in order to follow them over time. The area of each detection from one image to the next is compared. The Intersection Over Union (IOU) statistic is calculated for objects on two successive images. If the IOU is superior to a threshold, two detections on two successive images are considered as corresponding to the same object. An object can therefore be detected from the moment it is visible on the surface to the moment it leaves. Figure 3 is an example of successive detections of an object on the surface of the propellant.

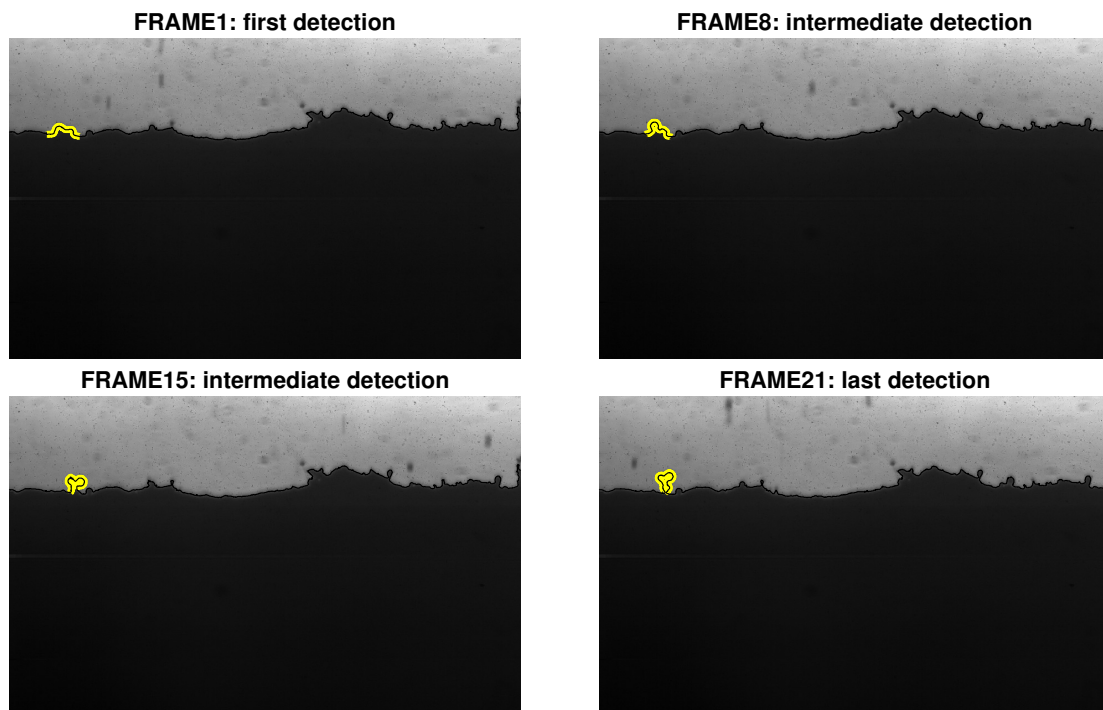


Figure 3: Example of the evolution over time of an object on the surface, automatically associated from one image to the other.

The detection of particles and aggregates in the gas flow is obtained by the MSER (Maximally Stable Extremal Regions)

AGGLOMERATION IN SOLID PROPELLANTS LOADED WITH INERT PARTICLES

algorithm [28], that was found very effective in the past for similar shadowgraphy images [25]. A relative size is estimated as an equivalent diameter depending on the area detected by MSER and the blur of the object. Individual particles are discriminated from aggregates depending on the size of the object and its aspect ratio using an SVM (Support-Vector Machine) approach. Figure 4 shows an example of an aggregate and a particle as detected by the complete algorithm.

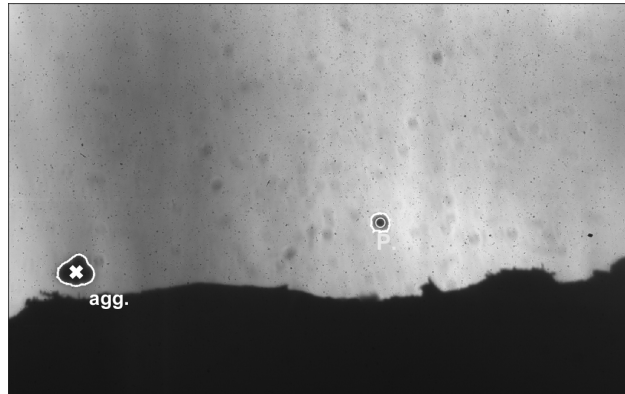


Figure 4: Example of a shadowgraphy image with two detections in the gas: one aggregate ('agg') and one single particle ('P').

A tracking of the objects in the gas flow was also developed. In the gas, the objects have a significant vertical displacement from one image to another unlike on the surface of the propellant, because of the vertical gas flow. The tracking is realized by calculating association scores between the detections in the gas flow on two successive images. In the current version, the score calculation is only based on two metrics: the distance between the barycenter of the detections, and the comparison between their respective areas.

3.3 Coupling detections on the surface to detections in the gas

Objects are detected on the surface over successive images, sometimes for several hundreds/thousands of images. In order to be sure that the last image corresponds to their release in the gas (and not a missed detection), confirmations of the object release are performed. Confirmations are made possible thanks to the detection of objects in the gas flow with MSER. A coupling of the detections in the two portions of the image (on the surface and in the gas flow) is carried out. Coupling validation is obtained by comparing the barycenter position for the last detection on the surface to the barycenter position of all detected objects in the gas flow on the following image. If the surface object is close enough for one gas object (as controlled by a threshold), the liberation of the surface object is validated. Figure 5 shows an example of such an association, an object leaves the surface and is detected in the gas flow on the following image.

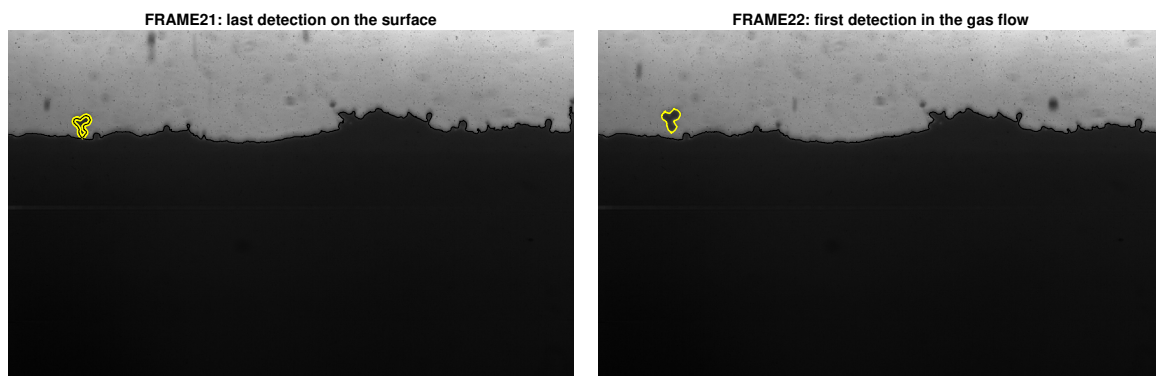


Figure 5: Example of detection association between surface detection and object detection in the gas.

The detections on the surface and in the gas flow are henceforth coupled. An object is now detected from its apparition on the surface to its exit from the image field. Two phases of an object's lifetime are visible on the recorded images: its uncovering as the propellant around it burns and its acceleration in the gas flow.

3.4 Particles and aggregates estimated metrics

Three calculated metrics provide quantitative information about the objects agglomeration in the solid propellant. The first is the size of the objects leaving the surface, investigating how pressure influence the particles agglomeration. The second is the residence time, investigating how objects are stuck more or less time on the surface, depending on several parameters such as pressure and the objects size. The third is the acceleration of the objects in the gas flow, representative of the object motion as a function of their size and gas velocity.

3.4.1 Representative size D_{eq}

A diameter is estimated for all the tracked objects on the surface and in the gas flow. The area of the object detected on the surface is not constant over time, since the early detections only correspond to a small portion emerging from the surface. The size of the surface object increases over time due to the regression of the surrounding propellant. The propellant around the object can mislead the area determined at each detection on the surface, depending on whether the propellant surface is plane or not. The detection in the gas flow is more accurate: the object real size is fixed (because it is inert) and it is surrounded by the gas flow, which is transparent. The equivalent diameter D_{equiv} is estimated as the diameter from a circle with the same area as the detected object :

$$D_{equiv} = 2 \sqrt{\frac{Area}{\pi}} \quad (1)$$

The blur in the gas flow is considered and corrected [23], making the diameter estimation more precise. The object diameter D_{eq} is estimated as the mean value of all the equivalent diameter D_{equiv} (with the blur corrected) of the track's N detections in the gas flow (from its ejection from the surface to the moment it is no longer visible on the image field).

3.4.2 Residence time τ

Residence time depends on two antagonist forces, a drag force by the gas flow and surface retention. A particle placed inside the propellant during its production is exposed progressively to the gas flow as the propellant burns. The gas flow pulls the object through a drag force depending on the area of the object uncovered from the solid propellant, i.e. the portion of the object above the solid propellant surface.

The surface retention applied to the object is little understood [29] and the adhesion mechanisms of particles at the burning surface are not well known. The object on the surface is subject to two opposite forces, the surface tension (force trying to stick the object to the surface) applied by the propellant and the drag force applied by the flow (force trying to eject the object from the surface). Their comparison rules whether an object sticks to the surface or is ejected into the gas. The study of the residence time is a way of investigating the behavior of the object and obtain insight on the forces at play.

For each tracked detection on the propellant surface whose liberation in the gas flow has been confirmed by coupling, a residence time τ is calculated. It is defined as the time difference between the moment it is liberated and the moment it is first detected. In order to avoid the consideration of false objects coming from the back of the propellant (the propellant surface is not perfectly flat), an object has to be detected at least 5 times on the propellant surface ($\approx 0.6ms$) to be considered.

3.4.3 Acceleration a

The second stage of an object lifetime is its acceleration in the gas flow, following its ejection from the propellant surface. The objects accelerations depends on the drag force according to Newton's laws of motion to study, this is very interesting for two reasons:

- The drag force is equal to the surface tension just before the ejection of the objects in the gas. Calculating the acceleration is a way to get back to the surface tension, being able to calculate this force would be great for aluminum agglomeration modelling [21].

- The particles and aggregates could be compared. Being able to model the drag force of the aggregates is an important concern in aluminum agglomeration modelling [21].

For particles

We start the analysis by focusing on particles, i.e. spherical objects of diameter D_p and velocity v_p in a gas flow of speed v_g . The drag force F is modeled by Stokes law (with the drag coefficient $C_d = \frac{24}{Re_p}$), valid for very low Reynolds numbers ($Re_p < 1$, valid here because of the very small particles and gas flow velocity in the range of m/s):

AGGLOMERATION IN SOLID PROPELLANTS LOADED WITH INERT PARTICLES

$$F = \frac{1}{2}\rho_g C_d A (v_g - v_p)^2 = 3\pi D_p \mu_g (v_g - v_p) \quad (2)$$

With ρ_g the gas volumetric mass density, A the cross sectional area and μ_g the gas dynamic viscosity. When gravity is neglected compared to the drag force, the equation of motion is then:

$$a_p = \frac{dv_p}{dt} = 18 \frac{\mu_g}{\rho_p D_p^2} (v_g - v_p) \quad (3)$$

With a_p the acceleration of the particle and ρ_p the particle volumetric mass density. The differential equation depends on the difference between the gas flow and the particle velocities. The time constant is $\tau_p = \frac{\rho_p D_p^2}{18\mu_g} \approx 20ms$ for the propellant studied. Objects in the gas flow are tracked for 15 frames at the most, the frame rate being $7500Hz$, they are tracked for 2ms or less. Because this time is far inferior to the time constant of the differential equation, the particle velocity can be neglected compared to the gas flow velocity. Therefore, the acceleration of the particle a_p in the gas flow can be assumed proportional to the inverse of the square of the diameter of the particle D_p and to the gas velocity v_g :

$$a_p \propto \frac{v_g}{D_p^2} \quad (4)$$

For aggregates

Aggregates are not spherical, they are several particles stuck together. The Reynolds number are still very low because of the small size of the objects. We model the drag coefficient $C_d(agg)$ as inversely proportional to the Reynolds number Re_{agg} but with another multiplying factor C_{agg} , depending on the aggregate shape:

$$C_d(agg) = \frac{C_{agg}}{Re_{agg}} \quad (5)$$

Therefore, the acceleration is also proportional to the inverse of the square of the aggregate relative size but with a different proportionality factor:

$$a_{agg} \propto C_{agg} \frac{v_g}{D_{agg}^2} \quad (6)$$

Position interpolation

Objects are tracked in the gas flow following their ejection from the propellant surface. The barycenter of the object (x_o, y_o) is determined for each detection. Only the vertical coordinate is considered for the acceleration calculation, the movement studied is only the vertical one following the gas flow. A distance to the propellant is also calculated, it is determined as the difference between the coordinate y_o to the coordinate y_s of the surface. y_s is calculated at the coordinate x_o of the first detection, i.e. the position of the surface below the center of the object: $y_s = surface_y(x = x_o)$.

The gas velocity is supposed constant at the first order, therefore the object acceleration should be relatively constant (eqs 4 and 6). The distance between the object and the surface should then be modelled by a 2^{nd} order polynomial function:

$$d(t) = y_o - y_s = d_0 + v_0 t + \frac{1}{2} a t^2 \quad (7)$$

The modelling provides the value of the initial distance d_0 , the initial velocity v_0 (which is very low) and the acceleration a .

4. Results

The three metrics exposed previously are calculated for each studied pressure. The residence time and the acceleration of the objects are first studied at atmospheric pressure. Then the effect of pressure is specifically studied.

4.1 Objects size distribution

The first focus is the size of the objects leaving the surface. The size repartition of the individual particles (non-agglomerated) is supposed to be pressure independent, i.e. the original repartition introduced in the propellant. The size repartition of the aggregates could possibly change, depending on the effect of pressure on agglomeration. If a pressure increase intensifies agglomeration (i.e. the number of particles agglomerated), the size of the aggregates will increase. Figure 6 is a cumulative histogram of the equivalent diameter for both particles and aggregates for the three different studied pressures (1, 3 and 10 bars).

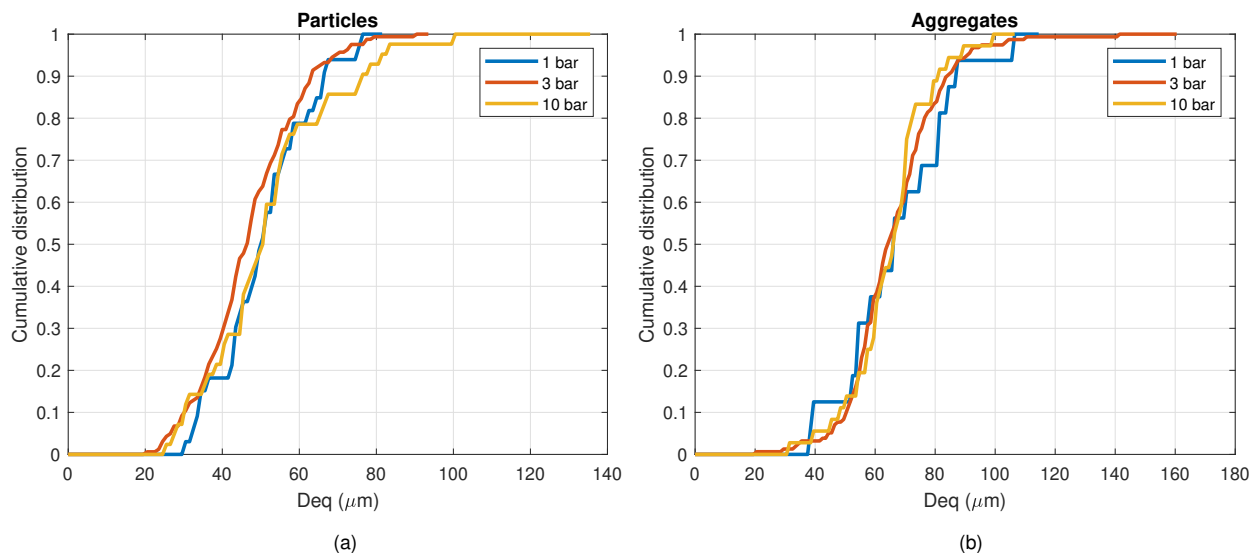


Figure 6: Particles and aggregates size distributions at the three pressure considered, for (a) particles and (b) aggregates.

The particles size repartition is not constant from one pressure studied to another. They are slightly shifted. The reason particles size repartition is not identical at the different pressure may be attributed to the blur correction. The images are more blurred with increasing pressure, affecting the MSER detection threshold and the subsequent blur correction. Still, the median particle diameter is around 40 μm for the three pressures. The median particle size of the initial particles introduced in the propellant is 34 μm , i.e. slightly smaller. This is consistent with an imperfect blur correction since blurred objects appear larger than they are. It might also be caused by the difficulty to detect and track smaller particles (below 15 μm). The aggregates size repartition is rather homogeneous at the different pressures, except for the smaller aggregates at 1 bar. If pressure has an influence on agglomeration, such as diminishing it, the aggregates size would diminish with pressure. A raw analysis would conclude that inert particles agglomeration does not vary with pressure. It will have to be investigated in more details in order to be sure that blur bias are not involved here. But it is important to remember that the blur bias affects more small objects, hence agglomerates should be less impacted.

4.2 Residence time

Figure 7 is a scatter plot of the residence time τ depending on the estimated diameter of the object for the test at atmospheric pressure. The y-axis is in log scale because of the large differences of residence times. Particles are plotted with blue circles and aggregates with red crosses.

The objects size does not seem to directly influence the residence time. If there were no surface tension applied by the propellant, the residence time would be linear to the objects size, which is not the case here. Some objects have residence time over 100 ms, the height of the surrounding propellant burned over that period is approximately 110 μm . This height is much larger than the size of the object, meaning the object is stuck on the surface while the propellant burns.

This deduction is useful in order to study agglomeration. An inert object is not necessarily ejected in the gas flow when the propellant around it is fully burned. It may be bound to the propellant for a certain time and go down with the supporting surface while the propellant material burns. This will have to be confirmed with more experimental data since the number of aggregates here remains limited.

AGGLOMERATION IN SOLID PROPELLANTS LOADED WITH INERT PARTICLES

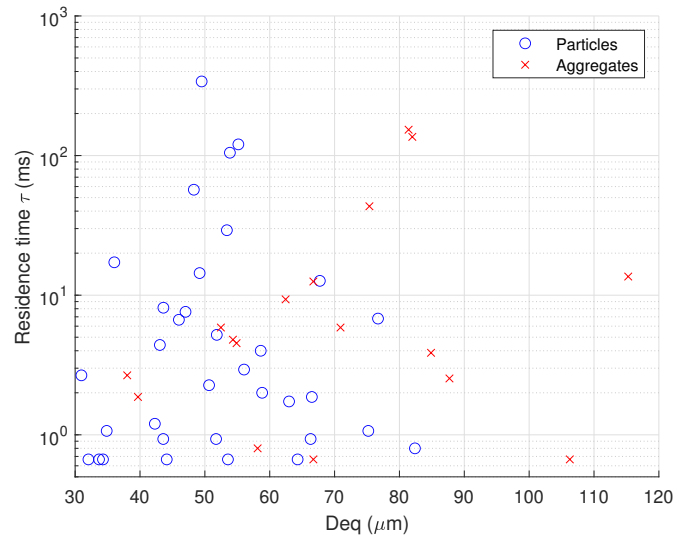


Figure 7: Scatter plot of the residence time depending on the size of the objects (at atmospheric pressure).

Pressure effect

A pressure increase leads to a burning rate increase, which means an object is uncovered more rapidly. We expect a decrease of the residence time with increasing pressure. Figure 8 is a cumulative histogram of the residence time τ of both particles and aggregates for the three different pressures studies (1, 3 and 10 bars).

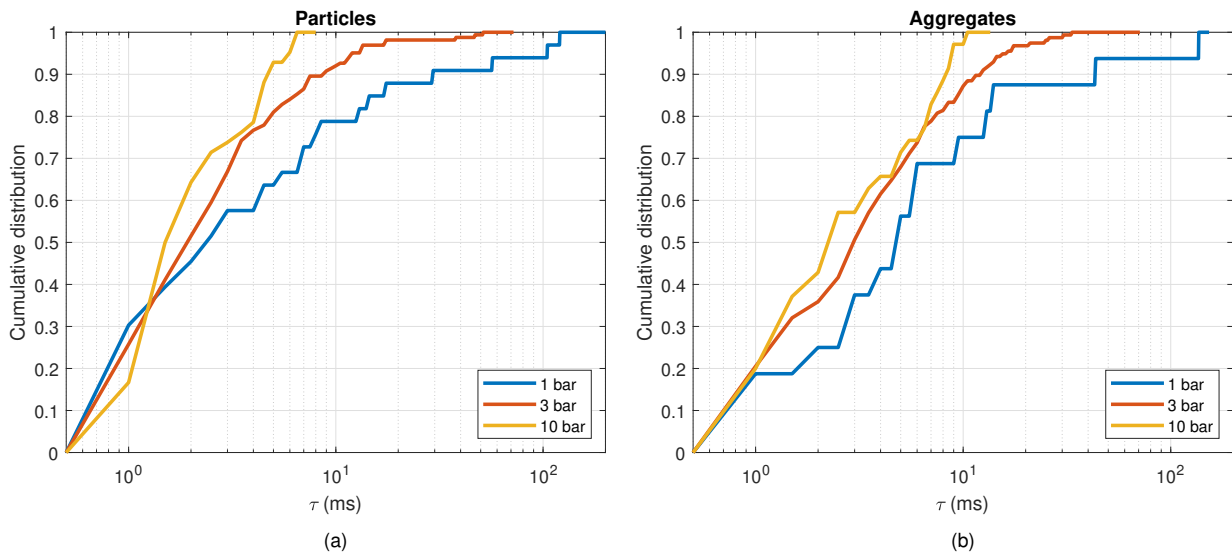


Figure 8: Cumulative histograms of the particles and aggregates residence time at the three pressure considered, for (a) particles and (b) aggregates.

As expected, the residence time decreases as the pressure increases. The study of the median residence time is insightful. Table 1 shows the median residence time of particles and aggregates $\tau_{med}(part)$ and $\tau_{med}(agg)$ at the three studied pressures. The burning rate is added, thus a representative height of propellant uncovered while the objects are on the surface can be calculated ($h_{med}(part)$ and $h_{med}(agg)$) thanks to the following equations.

$$\begin{aligned} h_{med}(part) &= r_b \tau_{med}(part) \\ h_{med}(agg) &= r_b \tau_{med}(agg) \end{aligned} \quad (8)$$

The median residence time τ_{med} decreases with pressure as previously exposed. However, the representative height

Table 1: Median residence time of particles and aggregates at the three pressure studied.

Pressure (bar)	1	3	10
$\tau_{med}(part)[ms]$	2.5	1.9	1.6
$\tau_{med}(agg)[ms]$	4.8	2.9	2.3
$r_b[mm.s^{-1}]$	1.17	2.98	4.40
$h_{med}(part)[\mu m]$	2.9	5.6	7.0
$h_{med}(agg)[\mu m]$	5.6	8.7	10

h_{med} of the uncovered propellant while the objects is stuck to the surface increases. It means that objects are more easily dragged in the gas flow at lower pressure. The reason can be attributed to gas velocity v_g . It can be estimated via mass conservation as:

$$v_g = \frac{\rho_{propellant} r_b}{\rho_g} \quad (9)$$

With $\rho_{propellant}$ the density of the solid-propellant sample. As a first approximation, the gas density ρ_g is directly proportional to pressure P (perfect gas law) and the burning rate follow a power law $r_b = AP^n$. Hence gas velocity varies with the following exponent:

$$v_g \propto P^{n-1} \quad (10)$$

n is generally comprised between 0.3 and 0.7, therefore the gas velocity always decreases with pressure. This explains why objects are ejected in the gas flow with a larger propellant height burned with increasing pressure. At higher pressure, the ejection of the object in the gas flow requires a larger portion of the object exposed to the gas flow in order to exceed the surface retention because of the slower gas. This is an interesting observation that might help estimate an order of magnitude for the surface retention force.

4.3 Acceleration in the gas flow

Figure 9 is the distance calculation $d(t)$ and interpolation of a particle following eq 7. Figure 9a shows the successive positions of the particle with representation of the barycenter calculated and the surface considered for the distance calculation. Figure 9b is a plot of the distance of the object to the surface as a function of time after its ejection in the gas flow. The blue symbols is the direct calculation of the position and the orange dashed line its modelling by a 2nd degree polynomial based on eq 7. Figure 10 is the distance calculation and modelling of an aggregate.

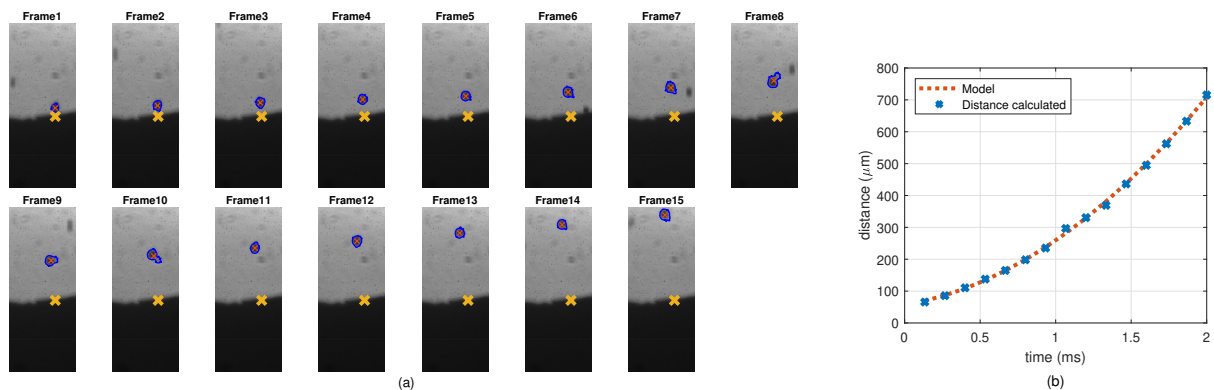


Figure 9: (a) Particle tracking. Particle barycenter are shown with red cross, surface position with orange cross. (b) Distance calculation and 2nd order interpolation.

The model seems to correctly fit the distance calculated ($r^2 = 0.999$ for the particle, $r^2 > 0.999$ for the aggregate). The acceleration a , the initial speed v_0 and the initial distance to the surface d_0 are obtained for all objects that have been detected on the surface and tracked in the gas flow. The speed of particles and aggregates can be determined using the following equation (derivation of the 2nd order interpolation for position):

AGGLOMERATION IN SOLID PROPELLANTS LOADED WITH INERT PARTICLES

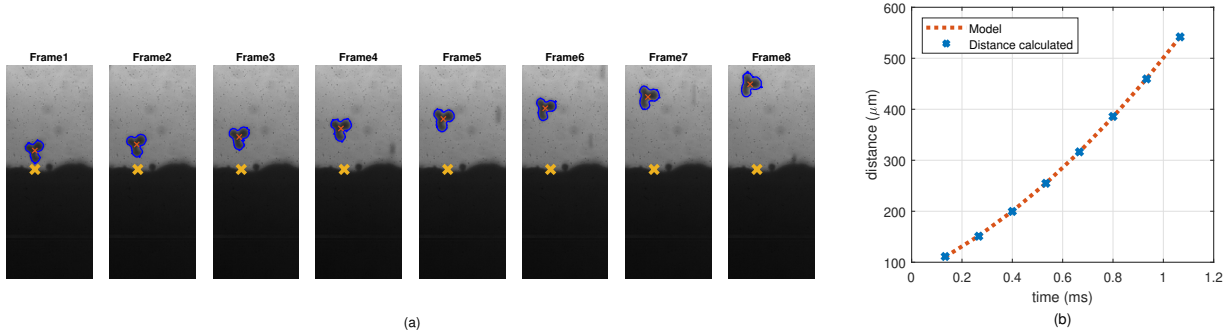


Figure 10: (a) Aggregate tracking. Aggregate barycenter are shown with red cross, surface position with orange cross. (b) distance calculation and 2nd order interpolation.

$$v(t) = v_0 + at \quad (11)$$

Figure 11 shows the velocity profiles for the particles and aggregates for the test at atmospheric pressure as estimated from the modelling. The x-axis corresponds to the velocity and the y-axis to the distance to the surface. For each figure, three mean velocity profiles are also plotted. They are determined using the mean initial distance to the surface of all the profiles ($d_{mean} = mean(d_0)$), the mean initial velocity ($v_{mean} = mean(v_0)$) and three representative values of the acceleration. Those three representative values are the median acceleration (solid line), the 25th percentile value and the 75th percentile value (dashed lines). The vertical variation of velocity is fairly consistent for all the individual profiles. The dispersion is attributed to the size distribution.

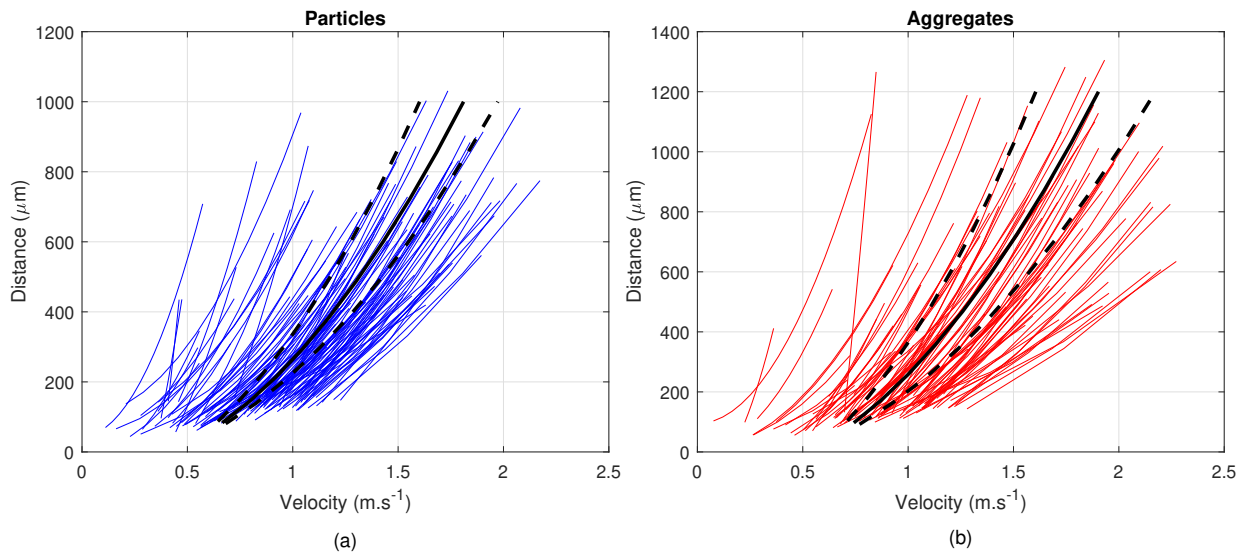


Figure 11: Velocity profiles of the (a) particles and (b) aggregates (at atmospheric pressure). Individual velocity profiles are in thin color lines, mean velocity profile in black solid line and velocity profiles for the 25th and 75th percentile in black dashed lines.

Pressure effect

We have previously seen that the acceleration a is expected to be proportional to the gas flow velocity: $a \propto \frac{v_g}{D^2}$. The gas velocity depends on pressure as previously exposed: $v_g \propto P^{n-1}$, with $n < 1$. As v_g decreases with pressure, the objects acceleration is expected to decrease as well. Figure 12a shows the mean velocity profiles for individual particles at the three pressures studied: 1, 3 and 10 bar. The representative velocity profiles are plotted as previously, involving the mean value of the initial distance to the surface d_{mean} , the mean value of the initial velocity v_{mean} and the median value of the acceleration. Figure 12b is the same for aggregates

AGGLOMERATION IN SOLID PROPELLANTS LOADED WITH INERT PARTICLES

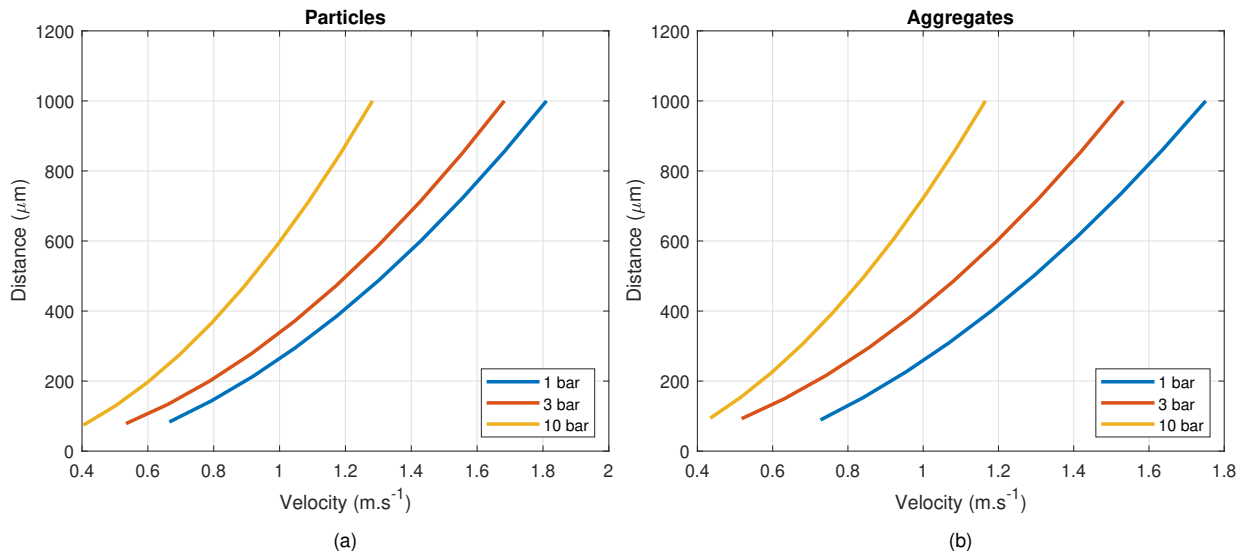


Figure 12: Set of representative velocity fields for (a) particles and (b) aggregates. The solid line is plotted using the median acceleration value.

As expected, the velocity is decreasing with increasing pressure. The acceleration is proportional to the gas velocity if the only force in the gas is the drag applied by the flow (Eq 2). As seen above with mass conservation, the gas velocity is proportional to P^{n-1} , or $\frac{r_b}{P}$. Figure 13 is a plot of the mean acceleration (as estimated from the 2^{nd} degree polynomial for position) as a function of ratio $\frac{r_b}{P}$ for the three pressure studied.

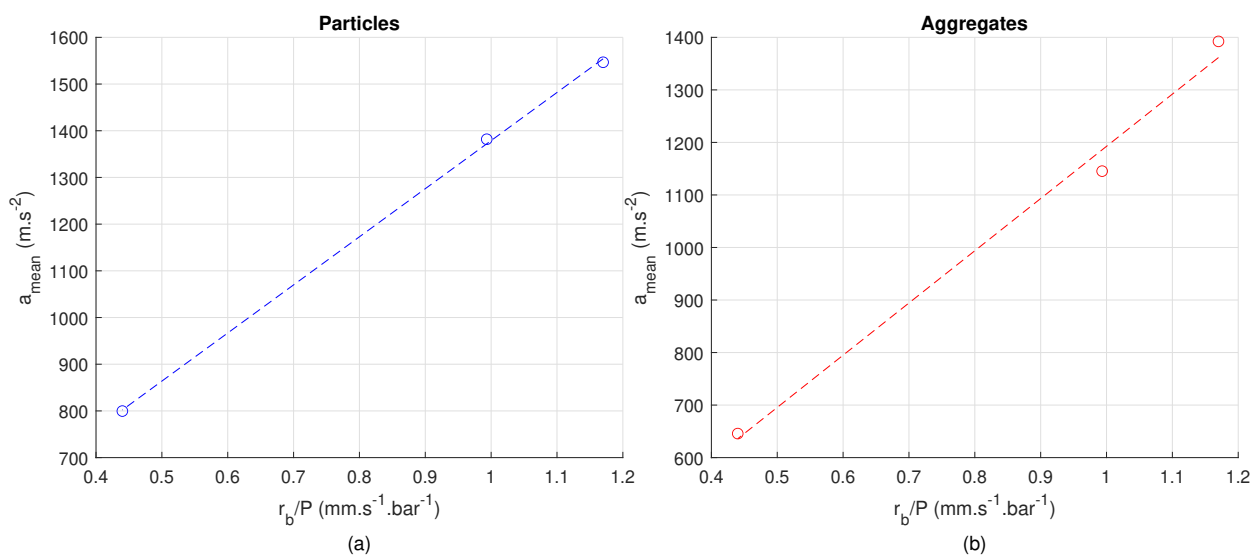


Figure 13: Scatter plot with a first degree interpolation of the mean acceleration depending on the ratio $\frac{r_b}{P}$ at the three different pressures, for (a) particles and (b) aggregates.

Figure 13 does show that the mean acceleration seems directly proportional to the ratio $\frac{r_b}{P}$. The trend is more evident for the particles ($r^2 = 0.999$), probably because of the similar shape for all the objects, compared to the various shapes possible for aggregates ($r^2 = 0.991$). The validation of the relation between acceleration and the gas velocity legitimizes the model of acceleration used here and confirms the good tracking of the objects in the gas flow. Adding data for more pressure will give more precision to the slope estimation, i.e. estimation of the drag force from the flow.

4.4 Analysis perspectives

Several dependencies have been exposed, such as the residence time dependence to pressure or the acceleration dependence to the ratio $\frac{r_b}{p}$. The next step for future studies is to validate the relation between the acceleration in the gas flow and the size of the object tracked. The size estimation has been proven to be very sensitive to the blur of the images, adding uncertainty that must be considered before trying to demonstrate the relation.

The study has been realized on a single propellant composition at three pressures. The analyses are planned to be performed on other propellants with various modifications such as AP size or particle size. The mechanism of solid propellant pockets defined in several studies [15, 19] could be investigated.

5. Conclusion

This article focused on agglomeration in a solid propellant composition containing inert particles via shadowgraphy image processing. One propellant composition has been studied at three different pressures. Particles and aggregates are tracked through the two phases of their lifetime: their uncovering at the surface of the propellant and their movement in the gas flow. A special coupling has been developed in order to associate the two phases of an object's lifetime.

Several physical analyses have been realized in order to investigate the behavior of the objects on the surface and in the gas flow. The results of those analyses can be used for future particles agglomeration models. Different metrics have been defined and calculated. On the surface, a residence time has been evaluated. It has been notably demonstrated that particles and aggregates were more easily ejected from the surface at lower pressure, the reason being the higher velocity of the gas flow.

In the gas flow, the acceleration of the objects has been estimated by modelling their distance to the surface over time. It was found that the acceleration is on average lower at high pressure. The reason is once again the decreasing gas flow velocity with increasing pressure. A deeper study of the objects acceleration could provide the retention force applied by the propellant when the objects are still on the surface.

6. Acknowledgements

We acknowledge the co-funding from ArianeGroup and ONERA for the present work.

References

- [1] E. W. Price and R. K. Sigman. "Combustion of aluminized solid propellants". *Solid propellant chemistry, combustion, and motor interior ballistics (Progress in Astronautics and Aeronautics)* 185 (2000), 663–687.
- [2] H. Cheung and N. S. Cohen. "Performance of solid propellants containing metal additives". *AIAA Journal* 3.2 (1965), 250–257.
- [3] G. P. Sutton and O. Biblarz. *Rocket propulsion elements, seventh ed.* Wiley, Hoboken, NJ, 2001.
- [4] M. Salita. "Deficiencies and requirements in modeling of slag generation in solid rocket motors". *J. Prop. Power* 11.1 (1995), 10–23.
- [5] N. Lupoglazoff et al. "Numerical simulations of the unsteady flow inside segmented solid-propellant motors with burning aluminum particles". In: *40th AIAA Aerospace Sciences Meeting & Exhibit*. 2002.
- [6] S. Gallier and F. Godfroy. "Aluminum combustion driven instabilities in solid rocket motors". *Journal of propulsion and power* 25.2 (2009), 509–521.
- [7] P. F. Pokhil et al. "Combustion of metal powders in active media". *Defense Technical Information Center, Technical Report AD0769576* (1972).
- [8] H. L. Churchill, R. W. Fleming, and N. S. Cohen. "Aluminum behavior in solid propellant combustion". *Lockheed Report* (1974).
- [9] P. L. Micheli and W. G. Schmidt. "Behavior of aluminum in solid rocket motors". *Aerojet Solid Propulsion Co* (1977).
- [10] J. K. Sambamurthi, E. W. Price, and R. K. Sigman. "Aluminum agglomeration in solid-propellant combustion". *AIAA J.* 22.8 (1984), 1132–1138.

AGGLOMERATION IN SOLID PROPELLANTS LOADED WITH INERT PARTICLES

- [11] M. W. Beckstead. “A Model for Solid Propellant Combustion”. In: *14th JANNAF Combustion Meeting, Baltimore, Maryland (USA)*. Vol. 1. 1977, pp. 281–306.
- [12] R. W. Hermesen. “Aluminum combustion efficiency in solid rocket motors”. In: *AIAA 19th Aerospace Sciences Meeting*. 1981.
- [13] M. Salita. “Survey of recent Al₂O₃ droplet size data in solid rocket chambers, nozzles, and plumes”. *31th JANNAF Combustion Meeting, Sunnyvale (USA)* (1994).
- [14] J. Duterque. “Experimental study of the agglomeration of aluminum in solid propellant motors”. *4th International Symposium on Special Topics in Chemical Propulsion, Stockholm (Sweden)* (1996).
- [15] N. S. Cohen. “A pocket model for aluminum agglomeration in composite propellants”. *AIAA J.* 21.5 (1983), 720–725.
- [16] V. G. Grigoriev, K. P. Kutsenogii, and V. E. Zarko. “Model of aluminum agglomeration during the combustion of a composite propellant”. *Combustion, Explosion and Shock Waves* 17.4 (1981), 356–363.
- [17] T. Jackson, F. Najjar, and J. Buckmaster. “A new class of agglomeration models for aluminum composite propellants based on random packs”. *J. Prop. Power* 21.5 (2005), 925.
- [18] V. Srinivas and S. R. Chakravarthy. “Computer model of aluminum agglomeration on burning surface of composite solid propellant”. *J. Prop. Power* 23.4 (2007), 728–736.
- [19] S. Gallier. “A stochastic pocket model for aluminum agglomeration in solid propellants”. *Propellants, Explosives, Pyrotechnics* 34.2 (2009), 97–105.
- [20] G. M. Knott, T. L. Jackson, and J. Buckmaster. “Random packing of heterogeneous propellants”. *AIAA journal* 39.4 (2001), 678–686.
- [21] M. Plaud and S. Gallier. “A numerical mesoscale model for aluminum agglomeration in solid propellants”. In: *7th European Conference for Aeronautics and Space Sciences, Milan (Italy)*. 2017.
- [22] R. W. Devillers et al. “Experimental analysis of solid-propellant surface during combustion with shadowgraphy images: new tools to assist aluminum-agglomeration modelling”. In: *7th European Conference for Aeronautics and Space Sciences, Milan (Italy)*. 2017.
- [23] M. Nogue. “Outils pour l’étude conjointe par simulation et traitement d’images expérimentales de la combustion de particules d’aluminium utilisées dans les propergols solides”. PhD thesis. Paris Saclay, 2019.
- [24] T. G. Decker, R. W. Devillers, and S. Gallier. “Detecting agglomeration patterns on solid propellant surface via a new curvature-based multiscale method”. *Measurement of Science Technology* (Submitted).
- [25] M. Nogue et al. “Particle detection & size evaluation in solid propellant flames via experimental image analysis to improve two-phase flow simulation in rocket motors”. In: *Space Propulsion*. 2018.
- [26] T. F. Chan and L. A. Vese. “Active contours without edges”. *IEEE Transactions on image processing* 10.2 (2001), 266–277.
- [27] F. Mokhtarian. “Silhouette-based occluded object recognition through curvature scale space”. *Machine Vision and Applications* 10.3 (1997), 87–97.
- [28] J. Matas et al. “Robust wide-baseline stereo from maximally stable extremal regions”. *Image and vision computing* 22.10 (2004), 761–767.
- [29] V. A. Babuk, V. A. Vasilyev, and V. V. Sviridov. “Formation of condensed combustion products at the burning surface of solid rocket propellant”. *Progress in Astronautics and Aeronautics Series* 185 (2000), 749–776.